

1 **Biodegradation, bioactivity and**
2 **biocompatibility analysis of plasma electrolytic**
3 **oxidized (PEO) biodegradable Mg implants**
4
5
6
7
8
9

10
11
12
13
14
15
16
17
18
19
20
21
22

ABSTRACT

In this paper, a plasma electrolytic oxidation (PEO) coating was prepared on AZ91 magnesium (Mg) implant to improve its degradation resistance, bioactivity and biocompatibility. The phase composition and surface morphology of the samples were characterized using X-ray diffraction (XRD) and scanning electron microscope (SEM). The corrosion rate and the bioactivity behavior of the samples were investigated via electrochemical measurements and immersion tests in simulated body fluid (SBF). The biocompatibility of samples was evaluated both *in vitro* and *in vivo*. To performed *in vitro* examinations, L-929 cells were cultured on both coated and uncoated substrates, and for the *in vivo* study, samples were implanted into the greater trochanter of rabbits as our animal model. The results showed that the PEO coating enhanced the corrosion resistance and *in vitro* and *in vivo* biocompatibility of AZ91 Mg implants.

23
24
25
26
27
28
29
30
31
32
33
34
35
36
37
38

Keywords: Plasma electrolytic Oxidation; Biodegradable Mg alloy; in vitro; in vivo; Biomedical applications

1. INTRODUCTION

Due to their strong mechanical properties, metallic implants have been widely used in bone treatment especially for large bone defects [1]. While they can help to hold bones in the proper position, metallic implants may become mobile and loose over time [2,3]. Also, they do not adjust with alterations in physiological conditions [4]. In some patients, the metal is rejected by the body or causes irritation to surrounding tissues [5]. In such cases, surgery may be required to remove the implants. However, there are potential complications from this type of surgery as the metal removal is not easy, especially with deep implants that have been in place for a long time. Moreover, removing the implant may lead to weakening of the bone where the implant was removed. To avoid such complications with metal implants, there are enormous endeavors to replace them by biodegradable polymers [6-9]. Biodegradability of such implants is a great advantage, as they will disappear after the bone heals. However, despite the advantages, commercially, metal implants are still preferred for large bone defects. This is due to the lack of mechanical strength of many biodegradable polymers as they may not be able to bear the load of the body [6-9]. Developing a biodegradable metallic implant can incorporate all these advantages.

39 Mg alloys can be one of the appropriate candidates for this purpose [10-12]. Mg is an
40 element essential to the human body and metabolism [13-16]. Mg alloys with good
41 mechanical characteristics, such as elastic modulus and yield strength that are closer to the
42 human bone tissue than other metallic implants, could minimize or avoid the stress shielding
43 effect caused by stainless steel or titanium alloys. The stiffness of Mg is about 40-45 Gpa.
44 Although that is larger than that of the bone, which is about 20-25 Gpa, it is much lower than
45 the stiffness of the other metallic implants such as stainless steel, cobalt alloy and titanium
46 alloy. Thus, it may work better in avoiding the stress shielding compared to other metals [17-
47 19]. However, Mg and its alloys are highly susceptible to corrosion in chloride-containing
48 solutions including human body fluid or blood plasma, which has restricted their clinical
49 applications [17, 20]. To be able to use Mg alloys in medical applications, it is crucial to
50 improve their corrosion resistance. Moreover, enhancing the bioactivity and biocompatibility
51 of Mg alloys is also necessary to improve the healing process [21]. Surface modification of
52 Mg alloys is a standard approach to decrease the corrosion rate and improve the bioactivity
53 and biocompatibility [22].

54 Recently, plasma electrolytic oxidation (PEO) coating has become an important
55 commercially applied protection method for some metallic alloys. During the PEO coating, a
56 plasma is produced and an oxide layer grows. The process involves melting, flow of the
57 melt, solidification, crystallization, partial sintering and densification of the growing oxide.
58 PEO coatings, are more stable and can inhibit corrosion better than chemical conversion
59 coatings [23,24]. To have the corrosion rate of Mg alloy around the bone self-healing rate,
60 release of the hydrogen gas should be below 0.01 ml/cm²/day [20]. In this case, the Mg alloy
61 is in biomedical grade and can be used for orthopedic applications. The AZ91 Mg alloy,
62 which we employed in this study, has around 0.01 ml/cm²/day hydrogen release. We
63 showed that the PEO coating can further decrease the corrosion rate of our Mg alloy, which
64 can improve the degradation and enhance the bioactivity and biocompatibility to facilitate the
65 bone treatment procedure.

66 In this study, the PEO coating was applied on AZ91 biodegradable Mg alloy and the
67 preparation, corrosion resistance, in vitro bioactivity, cytocompatibility and in vivo animal
68 study of the product are discussed.

69 **2. MATERIAL AND METHODS**

70 Plate samples (2×15×5 mm³) from an AZ91 Mg ingot were prepared in our laboratory. All
71 samples were ground with SiC emery papers of up to 600 grits, and then ultrasonically
72 cleaned in acetone for 20 min.

73 The PEO coating process was conducted on a direct current (DC) power supply. The
74 samples were used as the anode, while the stainless steel plate was the cathode. The
75 electrolyte for PEO coating treatment was composed of sodium silicate (200 g/L) and sodium
76 hydroxide (200 g/L). The distance between electrodes was 2 cm, time was 30 min and
77 voltage was 60V. Coated samples were cleaned ultrasonically with acetone after the
78 treatment and dried in air at room temperature.

79 The composition of the samples was characterized by X-ray diffraction (XRD, Philips X'Pert)
80 with a Cu k_α radiation in the 2θ range of 10-90°. Also, X-ray diffraction was derived from
81 coated flat specimen.

82 The surface morphology of the samples (before and after the immersion test) was analyzed
83 using a scanning electron microscope (Philips XL 30: Eindhoven) equipped with energy-
84 dispersive X-ray spectroscopy (EDS).

85 An Ametek potentiostat (model PARSTAT 2273) was used to perform the potentiodynamic
86 polarization and electrochemical impedance spectroscopy (EIS) tests. The samples were
87 used as the working electrodes. The test samples were rinsed with alcohol and then with
88 deionized water prior to the corrosion tests. A saturated calomel electrode (SCE) and
89 platinum electrode were used as the reference electrode and counter electrode, respectively.
90 Neutral (pH 7.4) simulated body fluid (SBF) was used as the corrosion test electrolyte. The
91 SBF is a standard solution, which has been used to assess the biocompatibility of potential
92 biomaterials. Thus, the behavior of samples was evaluated in the SBF to explore its
93 possibility of being used as a biodegradable implant material. The SBF was prepared
94 according to the procedures described by Kokubo and Takadama [25]. The polarization
95 curves of the test samples were measured with respect to the open-circuit potential at a scan
96 rate of 1.0 mV/s, and the EIS were measured over a frequency range from 100 kHz to 10
97 mHz. Before the polarization tests, the samples were kept in the solution for 1 hr to establish
98 the open circuit potential. The corrosion parameters, including corrosion potential (E_{corr}),
99 corrosion rate (I_{corr}), and polarization resistance (R_p), were obtained from the polarization
100 and EIS curves and were used to evaluate the corrosion resistance of the test samples.

101 The immersion test was carried out in the SBF. The samples were immersed in the SBF in
102 cylindrical bottles in a water bath at 37 °C. The volume of SBF for the immersion test was
103 used according to the following Eq. [25]:

$$104 \quad V_s = S_a/100 \quad (1)$$

105 where V_s is the volume of SBF (l) and S_a is the apparent surface area of sample (m^2).

106 The selected immersion periods were 0, 72, 168, 336, 504 and 672 hrs. After the pre-
107 selected immersion periods, the samples were dried at room temperature. For the in vitro
108 bioactivity evaluation, typical immersion morphology was characterized by SEM. Chromic
109 acid was used after the immersion in SBF to remove the corrosion products [26] and the
110 weight loss of samples was measured.

111 Cell culture test was performed using L-929 cell line. Dulbecco's modified Eagle's medium
112 (DMEM, Gibco) supplemented with 10% fetal bovine serum (FBS, Gibco), and 1% penicillin
113 streptomycin was used as the culture media. Cell viability and cell attachment examinations
114 were performed after 2, 5 and 7 days. For MTT assay analysis, we added 400 μl MTT to
115 each well and then replaced medium by 4 ml dimethylsulfoxide (DMSO). Cell viability was
116 measured by absorbance of the samples as $\text{OD}_{\text{sample}}/\text{OD}_{\text{negative control}} * 100\%$, where $\text{OD}_{\text{sample}}$
117 and $\text{OD}_{\text{negative control}}$ are the optical density of the sample and the negative control,
118 respectively. Cells attached on the samples were observed by SEM after fixing them on the
119 surface by 2.5% glutaraldehyde solution.

120 For the in vivo animal test, rod shape samples with 6 mm length and 3 mm diameter were
121 prepared. Rabbits with 3 kg weight were used for the surgery. The surgical procedure was
122 conducted according to the University Ethics Committee guidelines. AZ91 and PEO samples
123 were implanted into the greater trochanter of each rabbit. The X-ray radiography was taken
124 at the operation site 2 weeks after the surgery. In order to measure the changes of serum
125 magnesium, blood samples of about 1 mL were examined from the rabbits before the
126 implantation and at 2 weeks, 1 and 2 months of post-implantation and were analyzed using a
127 Hitachi 911 automatic hemocyte analyzer at the clinical & anatomical pathology laboratory.
128 The rabbits were scarified after 2 months and the new bone formation was seen by
129 histological images under a light microscope.

130

131 **3. RESULTS AND DISCUSSION**

132 Fig. 1 presents the SEM morphology of the PEO coating in low (a) and high (b)
 133 magnifications, and the XRD pattern from AZ91 substrate and PEO sample (c). The surface
 134 illustrated in Fig. 1a, b showed rough areas with some pores. This structure was formed by
 135 the molten oxide and gas bubbles, which were emitted out of the plasma arc dis-charge
 136 channels. According to Fig. 1b and XRD patterns in Fig. 1c, the PEO chemical structure was
 137 mainly composed of a mixture of Mg, MgO and Mg₂SiO₄ due to a series of reactions at
 138 strong electrical field and in a high temperature environment during the PEO coating
 139 process. Adjustment of PEO parameters, such as the electrolyte concentrations, current
 140 density, voltage and time, strongly affects the degree of thickness, porosity and quality of the
 141 PEO layer.

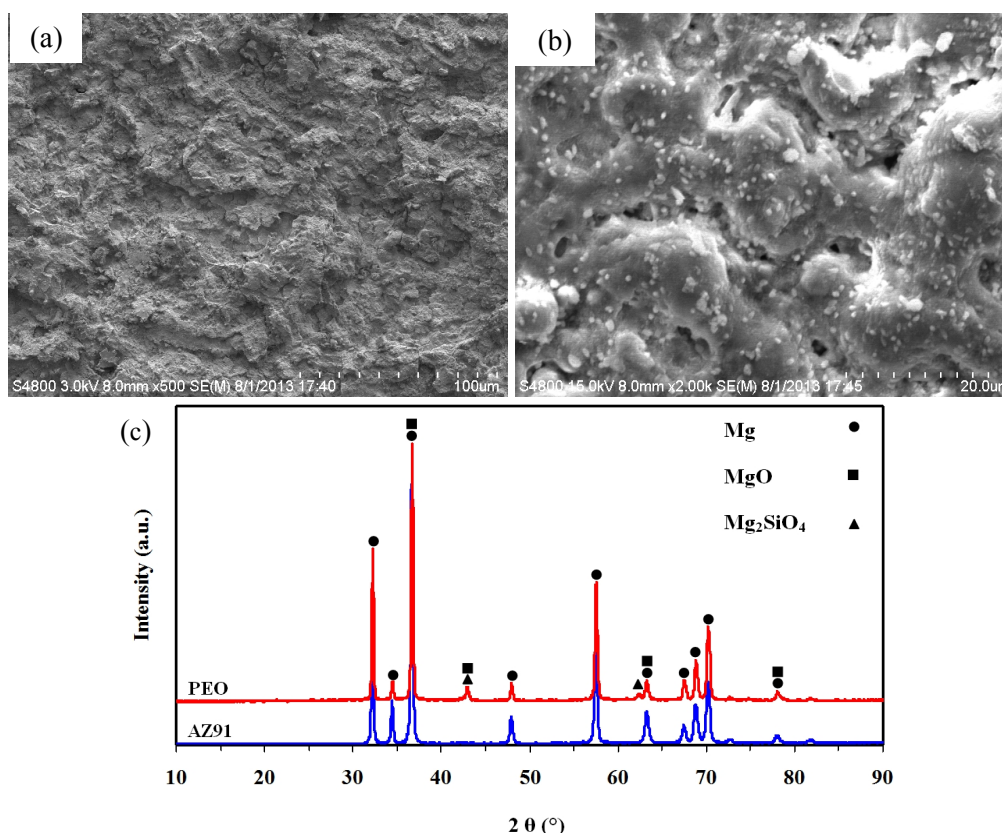
142

143

144

145

146



147

148

149 **Fig. 1. SEM morphology of the PEO coating in low (a) and high (b) magnifications, and**
 150 **the XRD pattern from AZ91 substrate and PEO sample (c) showing the morphology**
 151 **and composition of PEO coating.**

152 3.2. Electrochemical test

153 In order to evaluate the protection provided by PEO coating, potentiodynamic polarization
154 experiments and electrochemical impedance spectroscopy (EIS) measurements were
155 performed for the AZ91 and PEO coating. Fig. 2 shows the potentiodynamic polarization
156 curves (a) and EIS plots (b) of the AZ91 and PEO coating in the SBF. The electrochemical
157 corrosion parameters of the AZ91 and PEO coating were summarized and listed in Table 1.
158 Generally, the cathodic polarization curve represents the cathodic hydrogen evolution while
159 the anodic one represents the dissolution of Mg. Table 1 summarizes the corrosion potential
160 (E_{corr}) and corrosion current density (I_{corr}) obtained by Tafel extrapolation. As seen in Table 1,
161 it was found that the corrosion potential of the PEO coating is elevated slightly, while the
162 corrosion current density is reduced significantly, as compared to the AZ91 samples. As
163 shown in Table 1, regarding E_{corr} (vs. SCE) values we have PEO coating (-1.56 V) > AZ91 (-
164 1.6V) while about I_{corr} values: PEO coating (53700 nA/cm²) < AZ91 (63100 nA/cm²).
165 Therefore, the E_{corr} value of the PEO coating is less negative than that of the AZ91 sample
166 and the I_{corr} value for the PEO coating is much lower as compared to the AZ91 sample,
167 indicating that the PEO coating is less susceptible to corrosion.

168 EIS spectra further confirm the above point. According to the EIS plots, noticeable change
169 can be found due to the presence of the PEO coating. The capacitance loop diameters of
170 the PEO coating were larger than that of the AZ91 sample. In addition, the AZ91 sample
171 shows a much lower Z_{re} value compared to the PEO coating. For simplicity and for the sake
172 of comparison, one might approximately take the real impedance at which the imaginary part
173 vanishes for the capacitive part to be the polarization resistance R_p , and regard it as a
174 measure of corrosion resistance [26]. In the high frequency region, the impedance is
175 independent of the frequency, which is the resistance of the electrolyte between the sample
176 and the reference electrode. At the low frequency limit, the impedance is attributed to the
177 polarization resistance of the sample in the electrolyte. According to EIS data from Nyquist
178 plots regarding R_p values (Table 1), we have PEO coating (957.2 ohm) > AZ91 (305.5 ohm).
179 Based on the principle of corrosion electrochemistry, the low corrosion current density, high
180 corrosion potential, and high polarization resistance are proportional to good corrosion
181 resistance [27]. Since the corrosion of biodegradable Mg alloys is highly problematic in
182 biomedical applications [17], surface modifications are necessary to enhance the corrosion
183 resistance of these alloys in biological environments. The corrosion test results of this study
184 indicate that the corrosion resistance of AZ91 biodegradable Mg alloys was significantly
185 increased by employing surface coating prepared by PEO method. In parallel with the
186 electrochemical experiments, the immersion test can provide additional information
187 regarding the corrosion resistance of the AZ91 and PEO coating for longer periods of time.

188

189

190

191

192

193

194

195

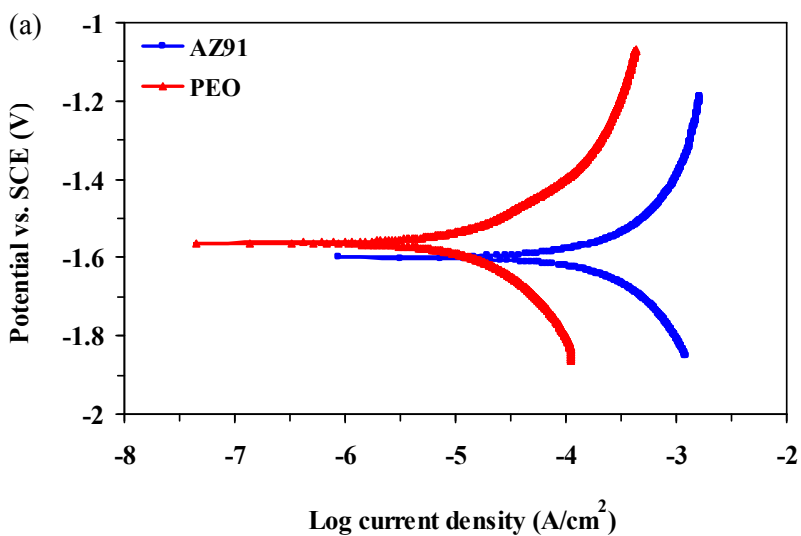
196

197

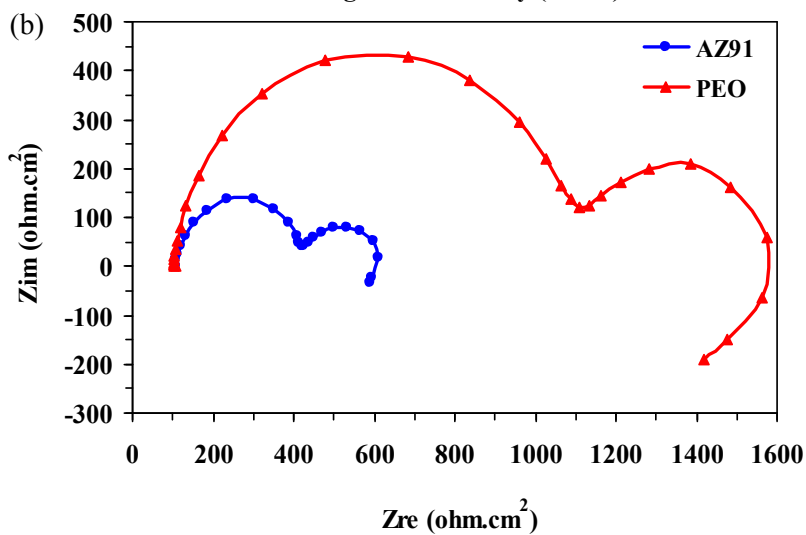
198

199

200



201



202

203

204 **Fig. 2. Polarization (a) and EIS (b) electrochemical tests for the AZ91 and PEO coating**
 205 **in the SBF showing the corrosion properties of uncoated and coated samples.**

206

207

208

209

210

211

212

213

214 **Table 1. Electrochemical corrosion parameters of the AZ91 and PEO coating derived**
 215 **from potentiodynamic polarization experiments and EIS measurements.**
 216

Samples	I_{corr} (nA/cm ²)	E_{corr} (V _{SCE})	R_p (ohm)
AZ91	63100	-1.6	305.5
PEO	53700	-1.56	957.2

217
 218

219

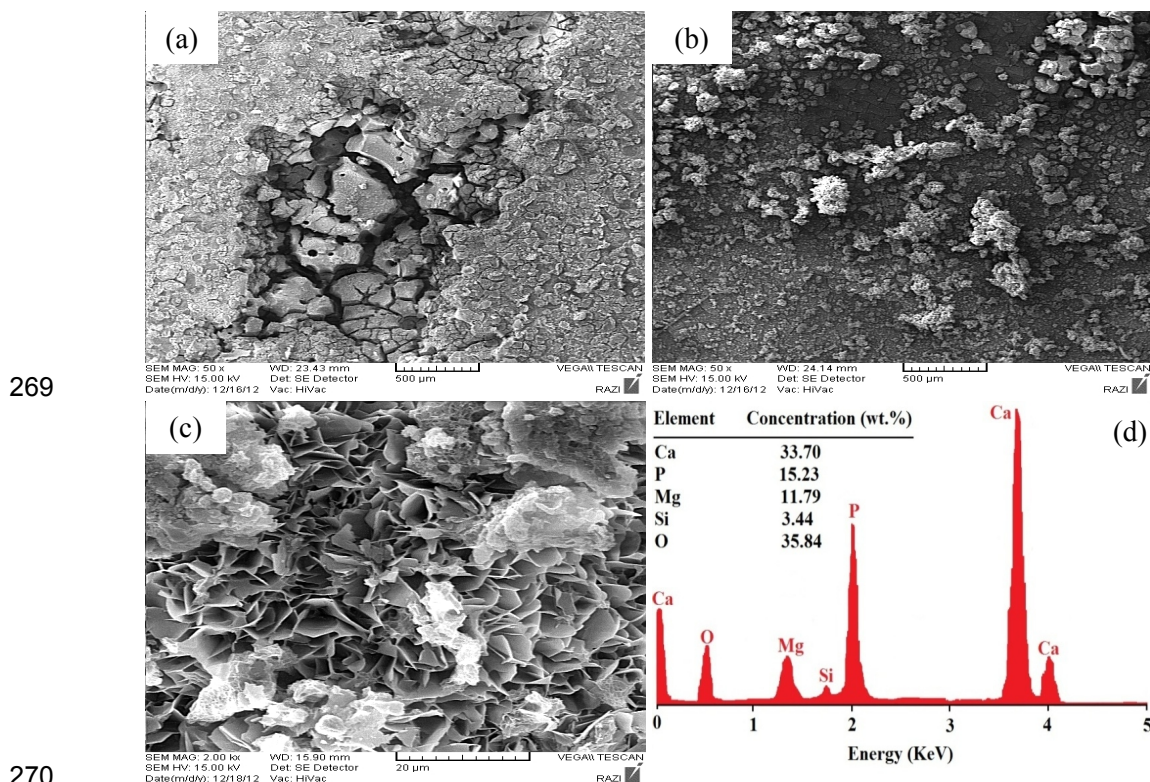
220 3.3. Immersion test

221 Immersion test was performed to observe the in vitro bioactivity and corrosion behavior of
 222 the samples for investigating the protective effect of the coating in long periods of time. Fig.
 223 3 shows SEM morphology of the AZ91 (a), and PEO coating in low (b) and high (c)
 224 magnifications after 672 hrs immersion in the SBF and EDS analysis of precipitated particles
 225 in broccoli-like structure on the surface of PEO coating after 672 hrs immersion in the SBF
 226 (d). As can be seen in Fig. 3a, various areas of the AZ91 sample surface were damaged and
 227 many large and deep network-like cracks were left on the surface due to the corrosion.
 228 Several particles were also deposited on the AZ91 surface. It can be seen from Fig. 3b that
 229 the PEO coating surface morphology has been destructed and some pits and cracks
 230 appeared on the surface of the substrate. This indicates that the PEO coating has corroded
 231 during the immersion process. Moreover, particles were also deposited on the PEO coating.
 232 As can be seen in Fig. 3c, the SEM observations further indicate the broccoli-like structures
 233 on the surfaces of the PEO coating after 672 hrs immersion in the SBF solution. Comparing
 234 the corrosion and in vitro bioactivity between the AZ91 and PEO coating in different
 235 immersion times, the cracks and pits of AZ91 sample are more evident than those of the
 236 PEO coating. On the other hand, it could be observed from SEM images that the PEO
 237 coating were subjected to milder and more uniform corrosion attack than the AZ91 sample.
 238 This indicates that the degree of corrosion damage was reduced for the PEO coating
 239 compared with the AZ91 substrates, consistent with the electrochemical measurements.
 240 Moreover, in the immersion experiments, the PEO coating induced more rapid and denser
 241 precipitation of particles compared with the AZ91 substrates. EDS analysis on a square area
 242 of precipitated particles in broccoli-like structure on the surface of PEO coating after 672 hrs
 243 immersion in the SBF, as shown in Fig. 3d, indicates that the precipitates were mainly
 244 composed of Ca, P, Mg, Si and O. Mg, Si and O elements existed in the MAO coating.
 245 However, Ca and P elements and also the broccoli-like structure can show the formation of
 246 bioactive minerals on the surface. It is known that the bioactive precipitates have a chemical
 247 composition close to the natural bone, which is an indication of good bioactivity and
 248 osteoconductivity and is beneficial to increase the chances for formation of an
 249 osteointegrated interface after implantation [28-31].

250 In the case of Mg alloys, due to the formation of large amounts of H₂, increasing the reaction
 251 rate decreases precipitation of corrosion products (bone-like apatite or bioactivity) on the
 252 substrate. By PEO coating, in vitro bioactivity was increased by decreasing the hydrogen
 253 release. Moreover, forsterite (Mg₂SiO₄) in PEO coating may acts as the nucleation cites for
 254 apatite precipitation which can increase the bioactivity. Mg alloy is a very active alloy. When
 255 it is immersed in the SBF, Mg dissolves and turns into Mg²⁺ and releases H₂ [32]. At the
 256 same time, Ca(H₂PO₄)₂ has the potential to hydrolyze and the hydrolysis product brushite
 257 (CaHPO₄·2H₂O) will precipitate on the surface of the Mg alloy. During this process, Mg²⁺
 258 released from the Mg alloy could react with any negative ions in the SBF, such as PO₄³⁻ to

259 form bioactive minerals [33]. Note that the hydrogen bubbles resulting from the high
 260 corrosion of the substrate can be obstacles for the newly formed particles to attach to the
 261 AZ91 substrate [32]. Stability of the implants and favorable bone–implant interface are
 262 especially important during the period of bone remodeling. However, Mg alloys degrade too
 263 fast during the bone remodeling period [34], leaving gaps around the implants. Therefore, the
 264 major concerns in coating of Mg alloy implants are the bioactivity issue and how they can
 265 remain intact during bone remodeling. Our results indicated that the PEO coating has
 266 improved bioactivity and osteoconductivity, and can more effectively promote the early stage
 267 of bone growth and tissue healing.

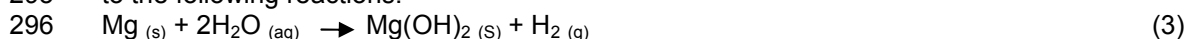
268



270
 271 **Fig. 3. SEM morphology of the AZ91 (a), and PEO coating in low (b) and high (c)**
 272 **magnifications after 672 hrs immersion in the SBF and EDS analysis of precipitated**
 273 **particles in broccoli-like structure on the surface of PEO coating after 672 hrs**
 274 **immersion in the SBF (d).**
 275

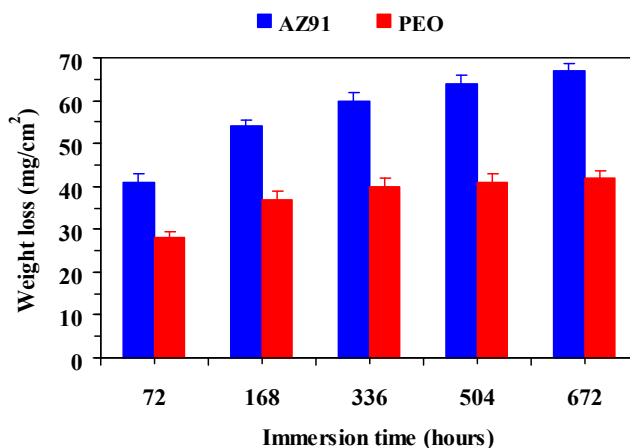
276 Fig. 4 shows the amount of weight loss of the AZ91 and PEO coating versus immersion time
 277 in the SBF. All samples presented a rapid increase in the weight loss at the first 72 hrs in all
 278 solutions, and then the weight loss increased gradually with the extension of immersion. In
 279 all intervals, the weight loss of AZ91 substrate was much higher than that of the PEO coating
 280 samples in the SBF solution. All samples underwent weight loss during the SBF soaking.
 281 The weight loss of the AZ91 samples resulted from the corrosion reaction of Mg while the
 282 weight loss of the PEO coating was attributed to both the dissolution of PEO coating and
 283 corrosion of the Mg substrate. The results of the immersion tests are consistent with those of
 284 the electrochemical measurements, indicating the effective protection provided by the PEO
 285 coating. Release elements during the corrosion of AZ91 include Mg, Al, Zn, and H₂. Mg

286 element is biocompatible and 450 mg Mg is allowed to be released daily in the 70 Kg human
 287 body [20]. During the corrosion of AZ91, the release rate of Mg is much lower than this
 288 criterion, even in the first days of corrosion. About Al and Zn, it is in the form of $Mg_{17}Al_{12}$ and
 289 $MgZn_2$ precipitates in the Mg matrix that are biocompatible [20]. The most important element
 290 is H_2 , which has influence on the adjacent tissues. Release of the H_2 gas should be below
 291 $0.01 \text{ ml/cm}^2/\text{day}$. The AZ91 Mg alloy, which we employed in this study, has below 0.01
 292 $\text{ml/cm}^2/\text{day}$ hydrogen release [20]. Overall, the AZ91 Mg alloy is biomedical grade. The
 293 release elements of PEO coating are MgO and Mg_2SiO_4 . MgO is a biocompatible [35], and
 294 Mg_2SiO_4 is a bioactive and biocompatible material [36]. The corrosion proceeded according
 295 to the following reactions:



298 Mg is a metal with a rapid corrosion rate due to its active position in the electromotive force
 299 (EMF) series. Once Mg alloys are immersed in the SBF, chemical dissolution combined with
 300 electrolyte penetration result in rapid corrosion of Mg alloys substrate. Magnesium hydroxide
 301 ($Mg(OH)_2$) on the surface of Mg alloys, from reaction (3), reacts with chloride ions in the
 302 SBF to form the soluble $MgCl_2$ as can be seen in reaction (4) [35]. Thereafter, the corrosion
 303 products layers, which mainly consist of $Mg(OH)_2$, gradually thicken and the amount of
 304 corrosion decreases by immersion time. Although $Mg(OH)_2$ forms on the surface of Mg
 305 alloys, unfortunately, this layer is too porous to effectively protect the substrate from
 306 corrosion. Thus, the system suffers from a continuous weight loss at the final stage, which
 307 leads to dissolution of the Mg alloy. Note that precipitation of corrosion products on the
 308 surface of samples immersed in the SBF solution not only improves the in vitro bioactivity
 309 but also decreases the weight loss rate, significantly [28-31].

310



311

312 **Fig. 4. The amount of weight loss of the AZ91 and PEO coating versus immersion time**
 313 **in the SBF.**

314

315 **3.4. Cell culture test**

316 Table 2 presents the relative cell viability (% of control) of L-929 cells after 2, 5, and 7 days
 317 of incubation on the AZ91, and PEO coating. Based on the Table, the cell viability on the
 318 PEO samples is higher compared to AZ91 sample where the amount of cell viability

319 increased from 70 % at 2 days incubation to 85 % at 7 days but for AZ91 sample, it changed
 320 from 50 % at 2 days incubation to 58 % at 7 days incubation.
 321

322

323

324

325 **Table 2. The relative cell viability (% of control) of L-929 cells after 2, 5, and 7 days of**
 326 **incubation on the AZ91, and PEO coating.**
 327

Cell viability (%)	AZ91	PEO
2 days	50 ± 3	70 ± 5
5 days	55 ± 5	80 ± 6
7 days	58 ± 7	85 ± 7

328

329

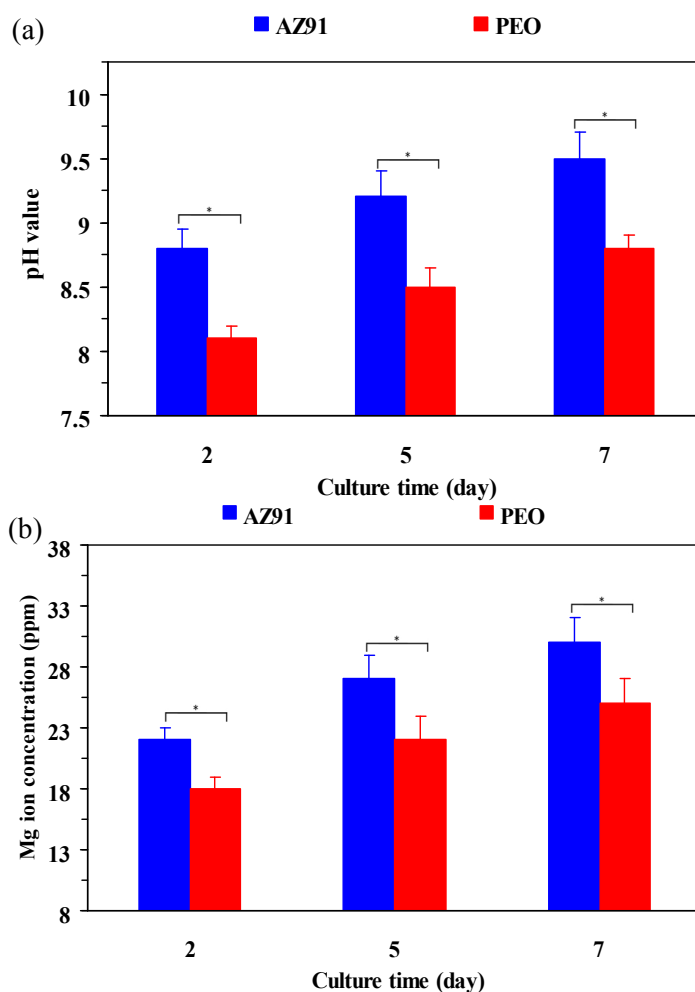
330 Fig. 5 presents the pH value (a), and Mg ion concentration of culture medium DMEM with L-
 331 929 cells (b) after 2, 5, and 7 days of incubation on the AZ91, and PEO coating. According to
 332 Fig. 7a, the pH increase of the PEO sample is slower than that of the AZ91 sample. The pH
 333 value of the AZ91 substrate increased to 8.8 and 9.5 after 2 and 7 days culture time,
 334 respectively. However, for the PEO sample it was 8.1 and 8.8 after 2 and 7 days,
 335 respectively. According to Fig. 7b, Compared to the AZ91 sample, the PEO coated samples
 336 present a much lower release of Mg ion. After 7 days, the Mg ion concentration for the PEO
 337 and AZ91 samples was 25 and 30 ppm, respectively. It is worth mentioning that the critical
 338 concentration of Mg ion for cytotoxicity is 40-60 ppm [37], and the Mg ion released from all
 339 samples in our study is under this amount. Cell viability depends on the cultural environment.
 340 For Mg alloys, the pH value and hydrogen evolution can adversely affect the
 341 cytocompatibility. The higher pH value and rapid hydrogen evolution results in less cell
 342 attachment, and then leads to less cell viability [38]. The PEO layer acts as a passive layer
 343 between the substrate and corrosive environment and reduces the degradation of the Mg
 344 substrate. This in turn slows down the pH increase and hydrogen evolution rate of the Mg
 345 sample. Hence, it creates a relatively stable interface for the cell adhesion and growth
 346 resulting in enhanced cytocompatibility.

347

348

349

350



351

352

353

354

355

356

357

358

359

360

361

362

363

364

365

366

367

368

369

370

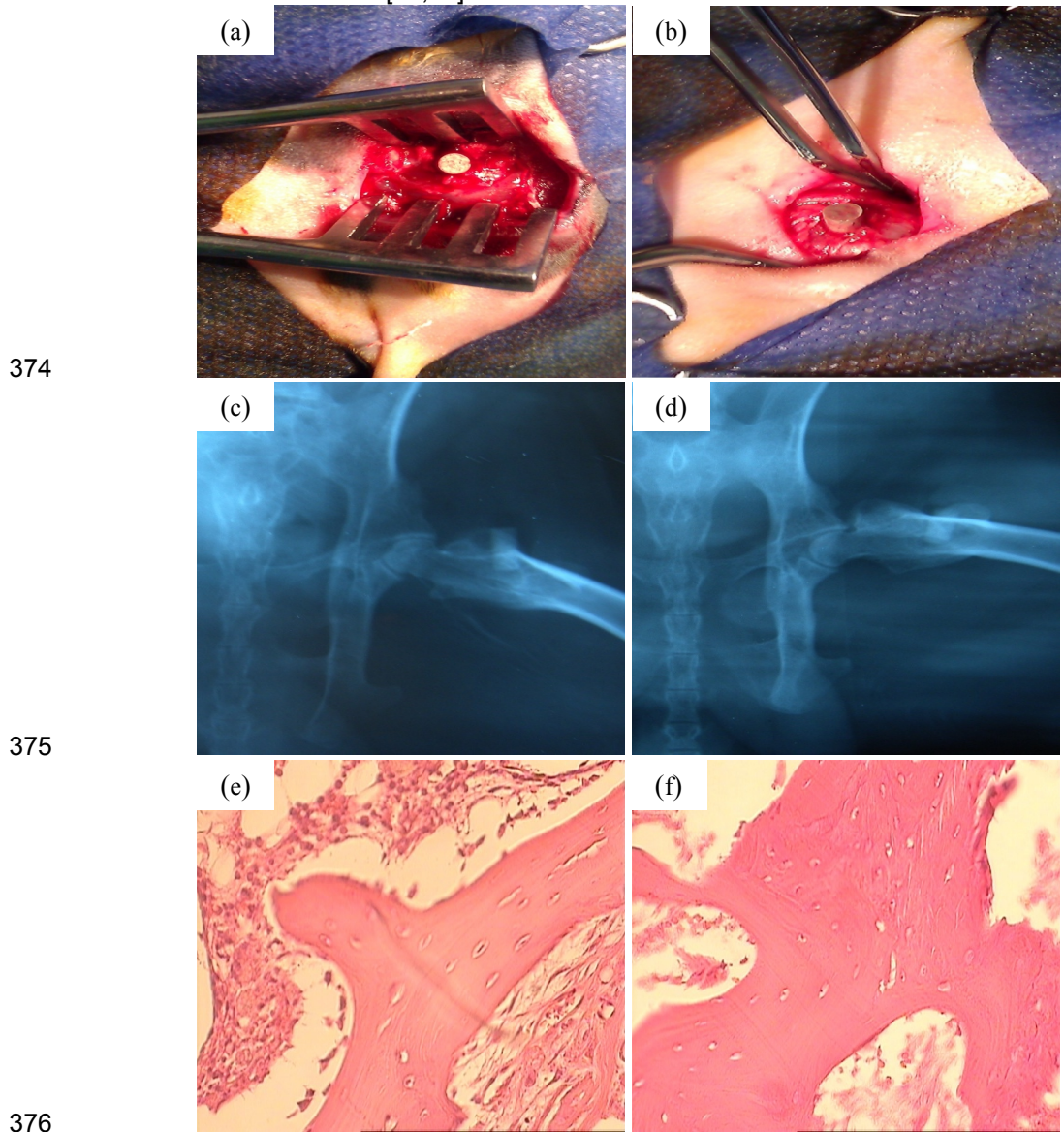
371

Fig. 5. pH value (a), and Mg ion concentration of culture medium DMEM with L-929 cells (b) after 2, 5, and 7 days of incubation on the AZ91, and PEO coating.

3.5. In vivo animal test

Fig. 6 shows the surgery images during the implantation of AZ91 (a) and PEO (b) implants, X-ray radiography images from AZ91 (c) and PEO (d) implants after 2 months implantation, and histological analysis of the bone surrounding AZ91 (e) and PEO (f) coated implants after 2 months post-operation. According to the X-ray radiography images, gas formation can be observed around the both implanted samples. However, the AZ91 sample shows more gas bubbles compared to the PEO sample due to its faster corrosion rate. According to the histological images, in comparing the amount of new bone formation, it was found that the uncoated AZ91 sample had the less amount of new bone formation than the PEO coated samples. Moreover, the amount of inflammation around the AZ91 implant was more than PEO implants. Also, new bone volume for the PEO coated implants are more compact and uniform than the AZ91 implants indicating that the coated Mg alloy implant is more compatible for bone growth at the early healing process. higher amount of bone formation and better quality around the PEO coated samples compared to the uncoated AZ91 samples can mainly due to the lower degradation rate which leads to slower hydrogen release, as

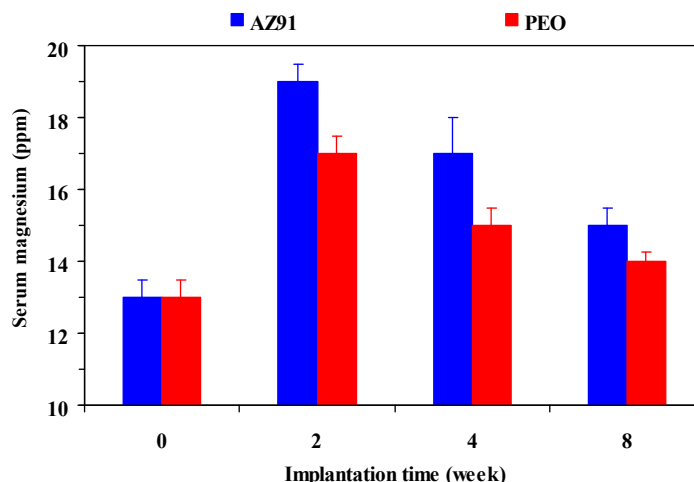
372 formation of hydrogen bubbles disturb the bone reaction and callus production, resulting in
 373 less new bone formation [39,40].



378 **Fig. 6. Surgery images during the implantation of AZ91 (a) and PEO (b) implants, X-ray**
 379 **radiography images from AZ91 (c) and PEO (d) implants after 2 months implantation,**
 380 **and histological analysis of the bone surrounding AZ91 (e) and PEO (f) implants after**
 381 **2 months post-operation.**

382

383 The serum magnesium in blood for AZ91 and PEO implants versus post-operation time is
 384 presented in Fig. 7. The serum magnesium of all rabbits at the time point 0 was the same,
 385 and after the implantation this value increased for all samples. The normal range of serum
 386 magnesium level is 20 ppm [41], and for all samples in our study, this value is below 20 ppm.
 387 Compared to the uncoated AZ91 samples, the amount was less in magnesium ions for the
 388 PEO coated implant before and after implantation, indicating that the in vivo biodegradation
 389 of the PEO coated implant did not induce a great increase of Mg ions.



390 **Fig. 7. The serum magnesium in blood for AZ91 and PEO implants versus post-**
 391 **operation time.**
 392

393
 394 The weight loss of implanted samples after 2 months post operation was measured and
 395 presented in Table 3. The weight loss of the PEO and AZ91 samples were 16, and 25
 396 mg/cm², respectively, which indicates the PEO implant has improved degradation resistance
 397 compared to the AZ91 sample.

398 **Table 3. The amount of weight loss for the AZ91, and PEO coated samples after 2**
 399 **months implantation.**
 400

sample	AZ91	PEO
Weight loss (mg/cm ²)	25	16

401

402
 403 **4. CONCLUSION**

404 The corrosion resistance, in vitro bioactivity and biocompatibility of biodegradable Mg alloy
 405 was increased by the Plasma electrolytic oxidation method.
 406

407 **ACKNOWLEDGEMENTS**

408 The authors are thankful for the contributions of Isfahan University of Technology,
 409 Torabinejad Dental Research Center, Oklahoma Center for Advancement of Science and
 410 Technology (Grant no. AR131-054 8161), AFOSR (Grant no. FA9550-10-1-0010) and the
 411 National Science Foundation (NSF, Grant no. 0933763).

412 **COMPETING INTERESTS**

413 Authors have declared that no competing interests exist.

414

415 **ETHICAL APPROVAL (WHERE EVER APPLICABLE)**416 All authors hereby declare that "Principles of laboratory animal care" were followed, as well
417 as specific national laws where applicable. All experiments have been examined and
418 approved by the appropriate ethics committee.

419

420 **REFERENCES**421 [1] Matsuno H, Yokoyama A, Watari F, Uo M, Kawasaki T. Biocompatibility and
422 osteogenesis of refractory metal implants, titanium, hafnium, niobium, tantalum and rhenium.
423 *Biomaterials* 2001;22:1253–1262.424 [2] Huiskes R, Weinans H, Vanrietbergen B. The relationship between stress shielding and
425 bone resorption around total hip stems and the effects of flexible materials. *Clin Orthop Relat*
426 *R* 1992;274:124–134.427 [3] Webster TJ, Siegel RW, Bizios R. Design and evaluation of nanophase alumina for
428 orthopaedic/dental applications. *Nanostruct Mater* 1999;12:983–986.429 [4] Piehler HR. Future of medicine. *Biomaterials* 2000;25:67–70.430 [5] Krecisz B, Kiec-swierczynska M, Bakowicz-mitura K. Allergy to metals as a cause of
431 orthopedic implant failure. *Int J Occup Med Environ Health* 2006;19:178–180.432 [6] Nejati E, Mirzadeh H, Zandi M. Synthesis and characterization of nano-hydroxyapatite
433 rods/poly(L-lactide acid) composite scaffolds for bone tissue engineering. *Comp Part A*
434 2008;39:1589–1596.435 [7] Lee SJ, Lim GJ, Lee J, Atala A, Yoo JJ. In vitro evaluation of a poly(lactide-co-glycolide)–
436 collagen composite scaffold for bone regeneration. *Biomaterials* 2006;27:3466–3472.437 [8] Fei ZQ, Hu Y, Wu, Wu H, Lu R, Bai J, Song H. Preparation and property of a novel bone
438 graft composite consisting of rhBMP–2 loaded PLGA microspheres and calcium phosphate
439 cement. *J Mater Sci: Mater Med.* 2008;19:1109–1116.440 [9] Zhao J, Guo LY, Yang XB, Weng J. Preparation of bioactive porous HA/PCL composite
441 scaffolds. *App. Surf. Sci.* 2001;255:2942–2946.442 [10] Witte F, Kaese V, Haferkamp H, Switzer E, Meyer–Lindenberg A, Wirth CJ, Windhagen
443 H. In vivo corrosion of four magnesium alloys and the associated bone response.
444 *Biomaterials* 2005;26:3557–3563.445 [11] Witte F, Fischer J, Nellesen J, Crostack HA, Kaese V, Pisch A, Beckmanne F,
446 Windhagen H: In vitro and in vivo corrosion measurement of magnesium alloys. *Biomaterials*
447 2006;27:1013–1018.448 [12] Xu LP, Yu GN, Zhang EL, Pan F, Yang K. In vivo corrosion behavior of Mg–Mn–Zn alloy
449 for bone implant application. *J Biomed Mater Res* 2007;83:703–711.450 [13] Klaue K, Fengels I, Perren SM. Long-term effects of plate osteosynthesis: comparison
451 of four different plates. *Injury* 2000;31:51–62.

- 452 [14] Wolf FI, Cittadini A. Chemistry and biochemistry of magnesium. *Mol Aspects Med*
453 2003;24:3–9.
- 454 [15] Rude RK. Magnesium Deficiency: A Cause of Heterogenous Disease in Humans. *J*
455 *Bone Miner Res* 1998;13:49–58.
- 456 [16] Rude RK, Gruber HE. Magnesium deficiency and osteoporosis: Animal and human
457 observations. *J Nutr Biochem* 2004;15:710–716.
- 458 [17] Staiger MP, Pietak AM, Huadmai J, Dias G. Magnesium and its alloys as orthopedic
459 biomaterials: a review. *Biomaterials* 2006;27:1728–1734.
- 460 [18] Saris NE, Mervaala E, Karppanen H, Khawaja JA, Lewenstam A. Magnesium: an
461 update on physiological, clinical, and analytical aspects. *Clin Chim Acta* 2000;294,1–26.
- 462 [19] Nagels J, Stokdijk M, Rozing PM. Stress shielding and bone resorption in shoulder
463 arthroplasty. *J Shoulder Elbow Surg* 2003;12:35–39.
- 464 [20] Song G. Control of biodegradation of biocompatible magnesium alloys. *Corros Sci*
465 2007;49:1696–1701.
- 466 [21] Song YW, Shan DY, Han EH. Electrodeposition of hydroxyapatite coating on AZ91D
467 magnesium alloy for biomaterial application. *Mater Lett* 2008;62:3276–3279.
- 468 [22] Razavi M, Fathi MH, Meratian M. Microstructure, mechanical properties and bio-
469 corrosion evaluation of biodegradable AZ91–FA nanocomposites for biomedical
470 applications. *Mater Sci Eng A* 2010;527:6938–6944.
- 471 [23] Razavi M, Fathi MH, Meratian M. Bio-corrosion behavior of magnesium–fluorapatite
472 nanocomposite for biomedical applications. *Mater Lett* 2010;64:2487–2490.
- 473 [24] Razavi M, Fathi MH, Meratian M. Fabrication and characterization of magnesium–
474 fluorapatite nanocomposite for biomedical applications. *Mater Charact* 2010;61:1363–1370.
- 475 [25] Kokubo T, Takadama H. How useful is SBF in predicting in vivo bone bioactivity?
476 *Biomaterials* 2006;27:2907–2915.
- 477 [26] Blawert C, Dietzel W, Ghali E, Song G. Anodizing treatments for magnesium alloys and
478 their effect on corrosion resistance in various environments. *Adv Eng Mater* 2006;8:511–
479 533.
- 480 [27] Chiu KY, Wong MH, Cheng FT, Man HC. Characterization and corrosion studies of
481 fluoride conversion coating on degradable Mg implants. *Surf Coat Technol* 2007;202:590–
482 598.
- 483 [28] Cui X, Li Y, Li Q, Jin G, Ding M, Wang F. Influence of phytic acid concentration on
484 performance of phytic acid conversion coatings on the AZ91D magnesium alloy. *Mater*
485 *Chemist Phys* 2008;111:503–507.
- 486 [29] Lee KY, Park M, Kim HM, Lim YJ, Chun HJ, Kim H, Moon SH. Ceramic bioactivity:
487 progresses, challenges and perspectives. *Biomed Mater* 2006;1:31–37.

- 488 [30] Li PJ, Kangasniemi I, Degroot K, Kokubo T. Bone-like hydroxyapatite induction by a
489 gel-derived titania on a titanium substrate. *J Am Ceram Soc* 1994;77:1307–1312.
- 490 [31] Larsen MJ, Pearce EIF. Dissolution of powdered human enamel suspended in acid
491 solutions at a high solid/solution ratio under a 5% CO₂ atmosphere at 20 °C. *Arch Oral Biol*
492 1997;42:657–663.
- 493 [32] Kouisni L, Azzi M, Zertoubi M, Dalard F, Maximovitch S. Phosphate coatings on
494 magnesium alloy AM60 part 1: study of the formation and the growth of zinc phosphate films.
495 *Surf Coat Technol* 2004;185:58–67.
- 496 [33] Feng B, Weng J, Yang BC, Qu SX, Zhang XD. Characterization of titanium surfaces
497 with calcium and phosphate and osteoblast adhesion. *Biomater.* 2004;25:3421–3428.
- 498 [34] Zhang Y, Yan C, Wang F, Li W. Electrochemical behavior of anodized Mg alloy AZ91D
499 in chloride containing aqueous solution. *Corros Sci* 2005;47:2816–2831.
- 500 [35] Hornberger H, Virtanen S, Boccaccini AR. Biomedical coatings on magnesium alloys –
501 A review. *Acta Biomater.* 2012;8:2442–2455.
- 502 [36] Kharaziha M, Fathi MH. Synthesis and characterization of bioactive forsterite
503 nanopowder. *Ceram Int* 2009;35:2449–2454.
- 504 [37] Zreiqat H, Howlett C, Zannettino A, Evans P, Schulze-Tanzil G, Knabe C, Shakibaei M.
505 Mechanisms of magnesium-stimulated adhesion of osteoblastic cells to commonly used
506 orthopaedic implants, *Biomed Mater Res*, 2002;62:175-184.
- 507 [38] Wong HM, Yeung KW, Lam KO, Tam V, Chu PK, Luk KD, Cheung K. A biodegradable
508 polymer-based coating to control the performance of magnesium alloy orthopaedic implants.
509 *Biomaterials* 2010;31:2084-2096.
- 510 [39] Serre C, Papillard M, Chavassieux P, Voegel J, Boivin G. Influence of magnesium
511 substitution on a collagen-apatite biomaterial on the production of a calcifying matrix by
512 human osteoblasts. *J Biomed Mater Res* 1998 (42) 626-633.
- 513 [40] Witte F, Kaese V, Haferkamp H, Switzer E, Meyer-Lindenberg A, Wirth C, Windhagen
514 H. In vivo corrosion of four magnesium alloys and the associated bone response.
515 *Biomaterials* 26 (2005) 3557-3563.
- 516 [41] Rettig R, Virtanen S. Composition of corrosion layers on a magnesium rare-earth alloy
517 in simulated body fluids. *J Biomed Mater Res Part A* 88 (2009) 359-369.

518
519
520
521